Research Article

ASFV transcription reporter screening system identifies ailanthone as a broad antiviral compound

Yuhang Zhang [a,1], Zhenjiang Zhang [b,1], Fan Zhang [c], Jiwen Zhang [b], Jun Jiao [c], Min Hou [c], Nianchao Qian [c], Dongming Zhao [b,*], Xiaofeng Zheng [a,*], Xu Tan [c,d,*]

[a] College of Veterinary Medicine, Hunan Agricultural University, Changsha 410128, China
[b] State Key Laboratory of Veterinary Biotechnology, Harbin Veterinary Research Institute, Chinese Academy of Agricultural Sciences, Harbin 150009, China
[c] Beijing Advanced Innovation Center for Structural Biology, Beijing Frontier Research Center for Biological Structure, MOE Key Laboratory of Bioorganic Phosphorus Chemistry & Chemical Biology, School of Pharmaceutical Sciences, Tsinghua-Peking Center for Life Sciences, Tsinghua University, Beijing 100084, China
[d] Institute of Health and Medicine, Hefei Comprehensive National Science Center, Hefei 230601 China

ARTICLE INFO

ABSTRACT

African swine fever (ASF) is an acute, highly contagious and deadly viral disease in swine that jeopardizes the worldwide pig industry. Unfortunately, there are no authoritative vaccine and antiviral drug available for ASF control. African swine fever virus (ASFV) is the etiological agent of ASF. Among the ASFV proteins, p72 is the most abundant component in the virions and thus a potential target for anti-ASFV drug design. Here, we constructed a luciferase reporter system driven by the promoter of p72, which is transcribed by the co-transfected ASFV RNA polymerase complex. Using this system, we screened over 3200 natural product compounds and obtained three potent candidates against ASFV. We further evaluated the anti-ASFV effects and proved that among the three candidates, ailanthone (AIL) inhibits the replication of ASFV at the nanomolar concentration ($IC_{50} = 15$ nmol/L). Our *in vitro* experiments indicated that the antiviral effect of AIL is associated with its inhibition of the HSP90-p23 cochaperone. Finally, we showed the antiviral activity of AIL on Zika virus and hepatitis B virus (HBV), which supports that AIL is a potential broad-spectrum antiviral agent.

1. Introduction

African swine fever (ASF) is an acute, highly contagious, and deadly viral disease affecting both domestic and feral swine of all ages with up to 100% case fatality rate. The outbreaks of ASF in China and central Europe in the summer of 2018 have greatly threatened the global swine industry (Zhou et al., 2018; Zhao et al., 2019). More than 43.46 million pigs succumbed to African swine fever virus (ASFV) infection or ASF-related impacts during the first year of the ASF outbreaks in China, the total economic loss caused by the ASF outbreak is estimated to be about US$ 111.2 billion (You et al., 2021). ASFV is the etiological agent of ASF, which is the only member of *Asfaviridae* family and the only known DNA arbovirus (Gaudreault et al., 2020). As one of the nucleocytoplasmic large DNA viruses (NCLDV), the ASFV genome is double-stranded DNA of 170–190 kb that encodes 150–200 viral proteins, including 68 structural proteins and more than 100 non-structural proteins (Alejo et al., 2018; Wang et al., 2019).

The structure of ASFV particle is composed of five layers: the external envelope membrane, the capsid, the inner membrane, the core shell and the inner core (Alejo et al., 2018; Wang et al., 2019). The major capsid protein, p72, is used for genotyping of ASFV strains because of its abundance and conservativeness (Ge et al., 2018). ASFV capsid comprises 8280 copies of major capsid protein p72 and 60 copies of penton protein. Three p72 molecules adopt a double jelly-roll structure to form one pseudo-hexameric capsomer, which is the unit that constitutes the majority of the mass of the viral capsid (Liu S. et al., 2019; Wang et al., 2019). Consequently, p72 not only accounts for 32% of the total mass of the virus particle, but also acts as one of the key capsomers during virus assembly (Liu Q. et al., 2019).

ASFV shares general characteristics of NCLDVs, for example, in addition to structural proteins, it also encodes proteins dedicated to the transcription and expression of its own genome (Alejo et al., 2018). About 20% of the ASFV genome encodes viral proteins responsible for the transcription and modification of its mRNA, which provides precise

spatial and temporal control of ASFV gene expression independent from the host transcription system (Dixon et al., 2013; Cackett et al., 2020; Zheng et al., 2022). There are at least 13 non-structural proteins related to virus transcription, including NP1450L, D205R, EP1242L, C147L, H359L, D339L, D1133L, Q706L, G1340L, B962L, B263R, C315R and I243L (Wang et al., 2021). ASFV RNA polymerase (RNAP) exhibits homology to the eukaryotic Pol II complex, for example, ASFV C315R is homologous to the TFIIB transcription factor which is in charge of the transcription initiation and RNAP-recruitment, and eight RNA polymerase subunits (NP1450L, D205R, EP1242L, C147L, H359L, D339L and CP80R) are involved in the transcription process (Cackett et al., 2020).

Currently, ASF outbreaks are still ongoing in China and several other countries and there are no widely approved vaccine and antiviral drug. Here, we report the establishment of a drug screening system consisting of a luciferase reporter driven by the promoter of p72 (p72-Fluc), which is transcribed by the co-transfected ASFV RNAP system. We screened over 3200 small molecule compounds using this system, which revealed that ailanthone (AIL), a quassinoid natural product, can significantly suppress ASFV replication. We also demonstrated that prostaglandin E synthase 3 (p23) is a key protein involved in the inhibitory effect of AIL, suggesting that the protein folding and maturation processes mediated by

p23 play an important role in ASFV replication. Our results imply that AIL targets p23 to disrupt the cochaperone cycle of heat shock protein 90 (HSP90), thus interfering the folding as well as the maturation of client proteins and impeding the expression of viral proteins. Additionally, we further evaluate the antiviral activity of AIL in Zika virus and hepatitis B virus, which indicates that AIL is a potential broad-spectrum antiviral agent.

2. Materials and methods

2.1. Cell culture and virus

Porcine alveolar macrophages (PAMs) were isolated from the lung lavage fluid of 4-week-old healthy specific pathogen free (SPF) piglets and maintained in RPMI-1640 medium (Gibco, USA, C11875500BT) containing 10% fetal bovine serum (FBS, PAN, Germany, P30-3033), 100 U/mL penicillin, 50 mg/mL streptomycin and non-essential amino acid (NEAA, Gibco, USA, 11,140,050). HEK293T and Vero-E6 cells obtained from ATCC were cultured in Dulbecco's Modified Eagle's medium (DMEM, Gibco, USA, C11995500BT) supplemented with 10% FBS. All mentioned cells were maintained at 37 °C with 5%
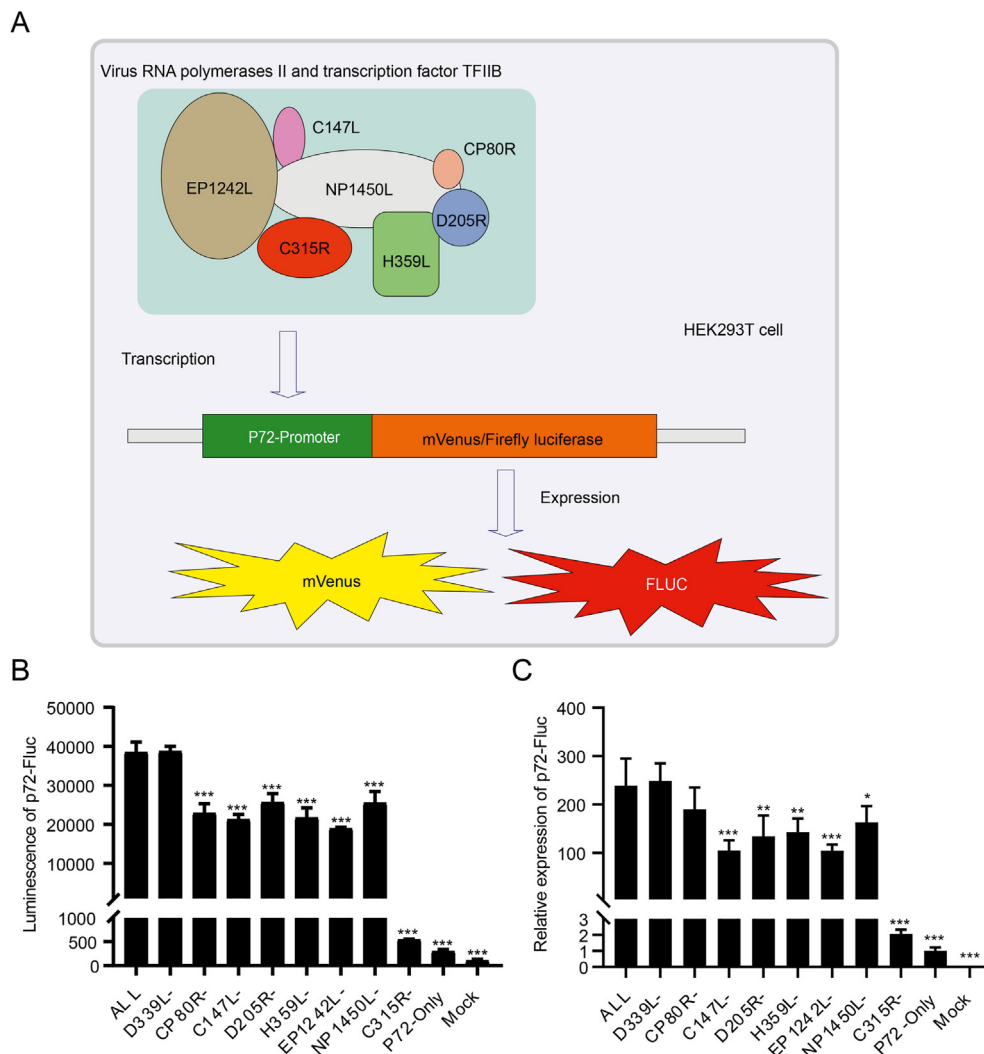

Fig. 1. Construction and verification of p72-Fluc reporter. **A** Schematic diagram of ASFV p72 promoter-driven luciferase reporter system. EP1242L, C147L, NP1450L, CP80R, D205R and H359L are reported subunits of ASFV RNA polymerase II system, C315R as a homologous analogue of the eukaryotic transcription factor TFIIB. HEK293T cells were transfected with p72-Fluc with or without certain ASFV polymerase and transcription factor II (C315R), the luminescence (**B**) and relative expression of p72-Fluc (**C**) were detected by luminometer and qPCR, respectively. Statistical significance is denoted by * $P < 0.05$, **$P < 0.01$, and ***$P < 0.001$.

CO_2. ASFV-eGFP strain (HLJ/18-6GD) was constructed and stored at Harbin Veterinary Research Institute (Chen et al., 2020). ASFV-HLG-2018 (GenBank: MK333180.1) was acquired from Harbin Veterinary Research Institute (Zhao et al., 2019). Zika virus (SZ01) stocks were prepared by propagation in C6 cells and titration by counting plaque-forming units (PFU) as described before (Li et al., 2018). Cell culture-derived HBV (ccHBV) viral stocks for HepG2-2B1 infection were obtained from the culture medium of HepAD38 cells (Xiang et al., 2019). All experiments with ASFV-eGFP and ASFV-HLJ-2018 were conducted within the enhanced biosafety level 3 (P3+) and level 4 (P4) facilities in the Harbin Veterinary Research Institute (HVRI) of the Chinese Academy of Agricultural Sciences (CAAS) approved by the Ministry of Agriculture and Rural Affairs.

2.2. Construction of plasmids and transfection

All constructs including p72-Fluc, D205R, C147L, CP80R, EP1242L, NP1450L, H359L, D339L, C315R, GFP and P23 were cloned into the PLX304, or EF1α- Flag lentiviral destinations via the Gateway cloning system (Invitrogen, USA, 11789021). For each transfection, Neofect (Biotech, China, KS2000) was combined with certain plasmids in Opti-MEM (Gibco, USA, 31985070) and added to cell media after 20 min incubation. At 6 h post-transfection, the media were refreshed with DMEM containing 10% FBS.

2.3. High throughput screening

HEK293T cells were transfected with plasmids of p72-Fluc system in 10 cm dishes and incubated for 8 h. The amounts of each plasmid were shown below: p72-Fluc 10 μg, C315R 4.5 μg, D205R 120 ng, EP1242L 120 ng, C147L 120 ng, CP80R 120 ng, NP1450L 120 ng, H359L 120 ng.

The cells were then reseeded to 96 well plates for another 8 h. Compounds from the BioBioPha natural product library were then added into the plates by the Echo® 550 liquid handler (Labcyte). At 24 h post-co-incubation, the activities of firefly luciferase were determined using the Luciferase Reporter Assay System (Promega Corporation, E1501) according to the manufacturer's instructions. Data were processed using Graphpad Prism and Excel. After conducting without transfected p72 system background subtraction, the fluorescence signal value (F) was normalized to Z-scores defined by $(F - F_{mean})/F_{sd}$, where F_{mean} and F_{sd} are the mean and standard deviation of drug-treated fluorescence signals at baseline, respectively.

2.4. Test of drug inhibition of ASFV-eGFP replication and hemadsorption assay

Cells were seeded into a 96-well plate (PAMs 2.5×10^5 cells/well; Vero 2×10^4 cells/well), and after the cells were completely adherent, fresh RPMI 1640 medium containing the drug was added to incubate for 2 h, and then ASFV-eGFP (MOI = 0.05) was inoculated for 2 h. Then, the cells were washed three times with PBS, and the RPMI 1640 medium within drug was added for 48 h at 37 °C, 5% CO_2. Finally, the brightfield and fluorescence pictures were taken with a fluorescence microscope.

The hemadsorption (HAD) assay was performed as described previously with minor modifications (Malmquist and Hay, 1960). Primary porcine peripheral blood monocytes were seeded in 96-well plates. The samples were then added to the plates and titrated in triplicate using 10 × dilutions. The quantity of ASFV was determined by the identification of characteristic rosette formation representing the haemadsorption of erythrocytes around infected cells. HAD was observed for 7 days, and 50% HAD doses (HAD_{50}) were calculated by using the method of Reed and Muench (1938).
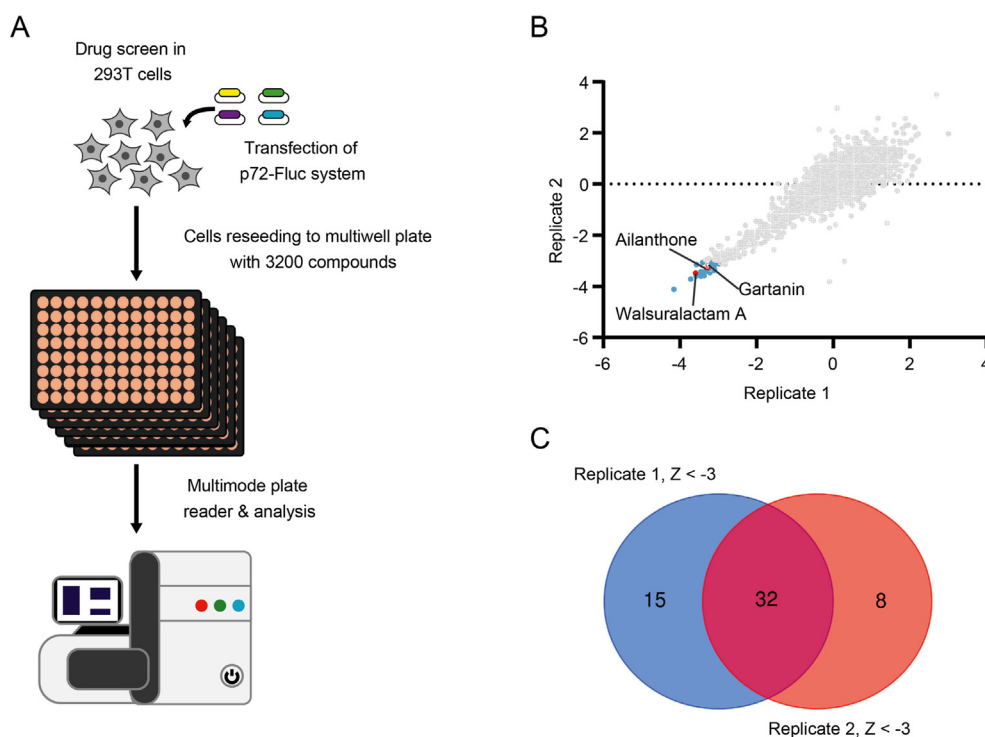

Fig. 2. Screening of drug libraries for compounds that inhibit p72-Fluc reporter. **A** Flow chart of high throughput screening. HEK293T cells were transfected with plasmids of p72-Fluc system and seeded in 96 well plates, afterwards, 3200 compounds were added into the plate by liquid handler, the luciferase intensity were read out by a microplate reader. **B** Standard scores analysis of high throughput screening results. The fluorescence signal value was normalized to Z-scores defined by $(F - F_{mean})/F_{sd}$, those candidates with values less than −3 were selected as potential hits. The intersection of the hits from the duplicate experiments is displayed by a Venn diagram (**C**).

2.5. Cell viability

Cell viability was detected by CCK8 kit (Beyotime, China, C0043) and CellTiter-Glo® Luminescent Cell Viability Assay (Promega, USA, G7571) according to the manufacturer's instructions. Here is a brief method for performing CellTiter-Glo assay: Vero cells were plated in 96-well plates and cells were incubated with drug for 24 h, then an equal volume of reagent was added to the wells containing cells and incubated for an additional 15 min. Finally, a luminometer is used to measure the luminescent signal, which is directly proportional to the amount of ATP present in the cell.

2.6. siRNA knockdown

The targeting sequences of siRNAs (si-P23) are listed in Supplementary Table S1. The transfection of siRNAs was performed with RNAimax (Invitrogen, USA, 13778030) or Celetrix Electroporation by following the manufacturer's instructions. Twenty-four hours after siRNA transfection, the cells were infected with ASFV at an MOI of 1.0 for 48 h siRNA knockdown efficiency of the target gene was assessed by RT-qPCR.

2.7. Quantitative real time-PCR

Total RNA from cells was extracted using a HiPure Total RNA Mini Kit (Magen, R4111-03) according to the manufacturer's instructions. The cDNA was generated by cDNA Synthesis Kit (Abm, USA, G490). The quantitative real-time PCR was performed with SYBR Green qPCR master mix (Vazyme, China, Q311-02) and data were detected by Bio-Rad CFX96 system (Bio-Rad). The expression of mRNA was assessed in each sample in triplicate, and GAPDH was used as an endogenous negative control. The expression of each target gene was calculated using the $2^{-\Delta\Delta CT}$ method. The primers for target genes are listed in Supplementary Table S2.

2.8. Western blot and ELISA

Cells were harvested and lysed in RIPA lysis buffer (Beyotime, China, P0013C) with a mixture of protease inhibitors (Biomake, USA, B14001). Samples were applied to 10% or 12% SDS/PAGE gels (Bio-Rad) and transferred to PVDF membranes (Millipore, USA, IPVH00010). Membranes were blocked with 5% nonfat milk in PBS with 0.1% Tween 20 and then probed with primary antibodies. The following antibodies were used in this study: anti-GAPDH (ZSGB-Bio, China, TA-08, 1:1000), anti-FLAG (Sigma, USA, F1084, 1:2000), anti-p72 and anti-p30 were made by Harbin Veterinary Research Institute (Zhao et al., 2019). The blots were developed by horseradish peroxidase reaction and imaged with a Protein-Simple FluorChem imaging system. Supernatants of cell media were collected to do ELISA experiment (SHANGHAI KEHUA, China, Diagnostic Kit for Hepatitis B e/s antigen).

2.9. Immunofluorescence imaging

Cells were fixed in 4% paraformaldehyde (PFA) for 15 min at 26 °C and permeabilized with 0.2% Triton X-100 for another 10 min at 26 °C. After washing three times with PBS, cells were incubated with diluted flavivirus group antibody (Genetex, China, GFX57154) for 2 h at 26 °C or at 4 °C overnight. Cells were then washed three times with PBS and incubated with Alexa Fluor conjugated secondary antibodies (Thermo-Fisher, USA, A11096) for an hour at 26 °C. After three washes in PBS, cells were then stained with DAPI (Solarbio). Images were captured using Olympus FV1000 confocal microscope (Olympus) or spinning disc confocal microscope (PerkinElmer or Andor). We used Volocity or ImageJ software for quantitative analysis.

2.10. Statistical analysis

Data were analyzed using GraphPad Prism 8.0 and presented as mean ± SEM unless stated otherwise. For data with two groups, student's t-test (paired, two-sided) was used. For data with more than two groups, a one-way analysis of variance (ANOVA) test was used, and appropriate adjustments were made for multiple hypothesis testing. P values are denoted as follows (ns: not significant, *$P < 0.05$, **$P < 0.01$, ***$P < 0.001$). Exact P values and statistical parameters are provided in Source Data File. All experiments were repeated at least three times unless otherwise stated.

3. Results

3.1. Construction of a p72 promoter-driven luciferase reporter

Luciferase reporter assays have been widely utilized for drug discovery due to their high sensitivity and robust signal. To report the transcription activity of ASFV RNAP, the promoter of the *p72* gene was constructed immediately upstream of the firefly luciferase gene (Fluc), once the virus polymerase binds to the promoter, the reporter can be transcribed to mRNA and finally luciferase can be expressed, which can be detected by a luminescence reader (Fig. 1A). There are eight RNA polymerase subunits of ASFV that have been reported, namely: NP1450L, EP1242L, H359L, D205R, C147L, D339L, C105R and CP80R, seven of them except C105R are evolutionary conserved in vaccinia virus (VACV), an extensively studied NCLDV (Cackett et al., 2020). We constructed a transcription system by expressing these seven polymerase subunits as well as a transcription factor C315R, which is responsible for the

Table 1
Cytotoxicity and IC$_{50}$ of 32 candidates.

Drug name	Cytotoxicity	IC$_{50}$ (μmol/L)	CC$_{50}$ (μmol/L)
Ailanthone	No	0.17	> 10
Walsuralactam A	No	2.5	> 10
Cedrelone	No	3	> 10
Gartanin	No	2.8	> 10
ent-6,9-Dihydroxy-15-oxokaur-16-en-19-oic acid β-D-glucopyranosyl ester	No	3	> 10
Rabdoternin F	No	6.8	> 10
1-Acetyltagitinin A	No	5	> 10
Chonglou Saponin VII	Yes	1.2345	1.433
Deoxylapacholssss	Yes	5.53	22.1
Methyl 2-(5-acetyl-2,3-dihydrobenzofuran-2-yl) propenoate	Yes	11.4	50.4
Valtrate	Yes	9.34	> 17.96
IVHD-valtrate	Yes	5.25	> 10.95
Picrasidine I	Yes	7.82	19.26
3″,4″-Di-O-acetyl-2″,6″-di-O-p-coumaroylastragalin	Yes	9.49	> 24.97
Dehydroherbarin	Yes	4.25	9.3
Bufotalin	Yes	0.72	0.72
8α-Acetoxyarglabin	Yes	No inhibition	> 10
Effusanin A	Yes	4.569	7.8276
Sprengerinin C	Yes	2.8901	3.8386
Uvedalin	Yes	2.881	4.8923
Cryptanoside A	Yes	0.57	#
2″-O-Acetylsprengerinin C	Yes	3.3186	3.3599
8β-Tigloyloxyreynosin	Yes	3.9057	5.7041
Ethyl (1-hydroxy-4-oxo cyclohexa-2,5-dien-1-yl) acetate	Yes	5.5454	5.8614
Epitulipinolide diepoxide	Yes	5.7702	6.6242
Sarmentocymarin	Yes	0.41	#
Thevebioside	Yes	0.46	#
Gliotoxin	Yes	1.47	1.47
alpha-Terthienylmethanol	Yes	1.7643	#
Arglabin	Yes	4.795	10.4872
Eriocalyxin B	Yes	1.0201	3.0087
Rubioncolin C	Yes	2.7347	5.092

"#" indicate the obvious cytotoxicity were observed with minimum concentration.

initiation and RNAP recruitment. The p72-Fluc were co-transfected with those elements with one of them removed to further evaluate this system. As expected, the luminescence was dramatically increased once the transcription system was added, and we detected a lower luciferase signal when any one subunit of RNAP or the transcription factor is removed except for D339L (Fig. 1B). The trends of mRNA expression levels were consistent with those of the luciferase assay (Fig. 1C). Compared to the group containing all the subunits, lack of D339L does not decrease the luciferase activity or mRNA expression, so we excluded the D339L from the transcription system. Taken together, these results demonstrated that the p72-Fluc system can mimic the transcription of p72 during ASFV infection.

3.2. Screening natural products that inhibit p72-Fluc system

Based on the p72-Fluc system, a natural product library (BioBioPha) was screened to identify potential compounds that can inhibit the expression of p72-Fluc (Fig. 2A). A total of 3200 compounds were screened in duplicate using the p72-Fluc assay in 96-well plate format. As shown with the Z scores calculated from the screening results, the duplicate experiments exhibited a strong correlation (Fig. 2B). Venn diagram shows the intersection of the two duplicate experiments yielded 32 potential candidates (Fig. 2C). The half-cytotoxicity concentration (CC_{50}) and half maximal inhibitory concentration (IC_{50}) of those candidates were further determined using follow-up dose titration experiments
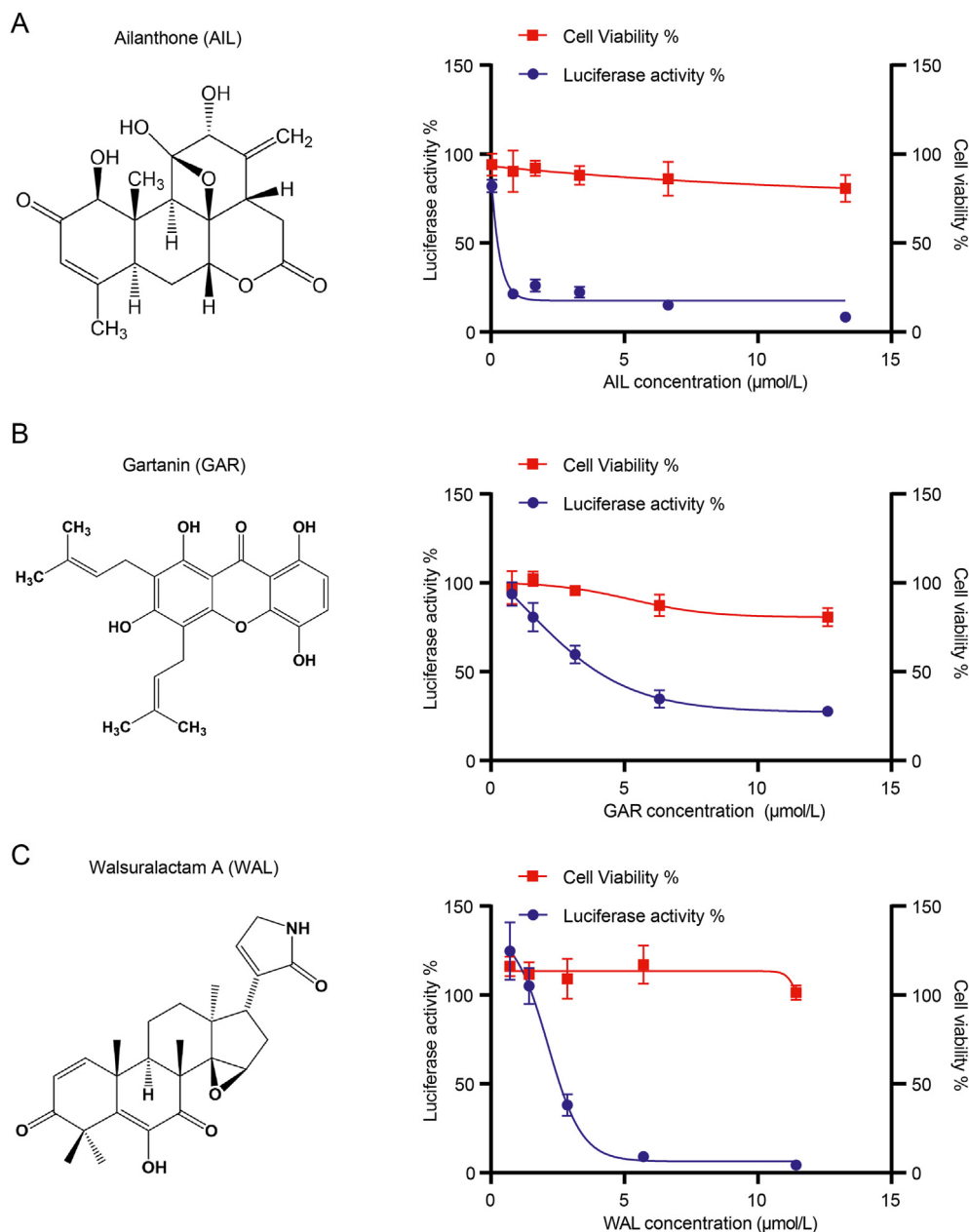

Fig. 3. Three candidates exhibited inhibitory effect on p72-Fluc. Chemical structure, luciferase activity and cell viability of AIL (**A**), GAR (**B**) and WAL (**C**). HEK293T cells (3×10^6) were seeded in 10 cm dish for 8 h incubation, then transfected with p72-Fluc system (the amount of each plasmids were shown below: p72-Fluc 10 μg, C315R 4.5 μg, D205R 120 ng, EP1242L 120 ng, C147L 120 ng, CP80R 120 ng, NP1450L 120 ng, H359L 120 ng), and then reseeded to 96 well plates for 6 h, followed by co-incubation with different concentrations of compounds as indicated for another 16 h. Luciferase activities were measured by luciferase reporter assay system, cell viability was detected by CCK8 kit.
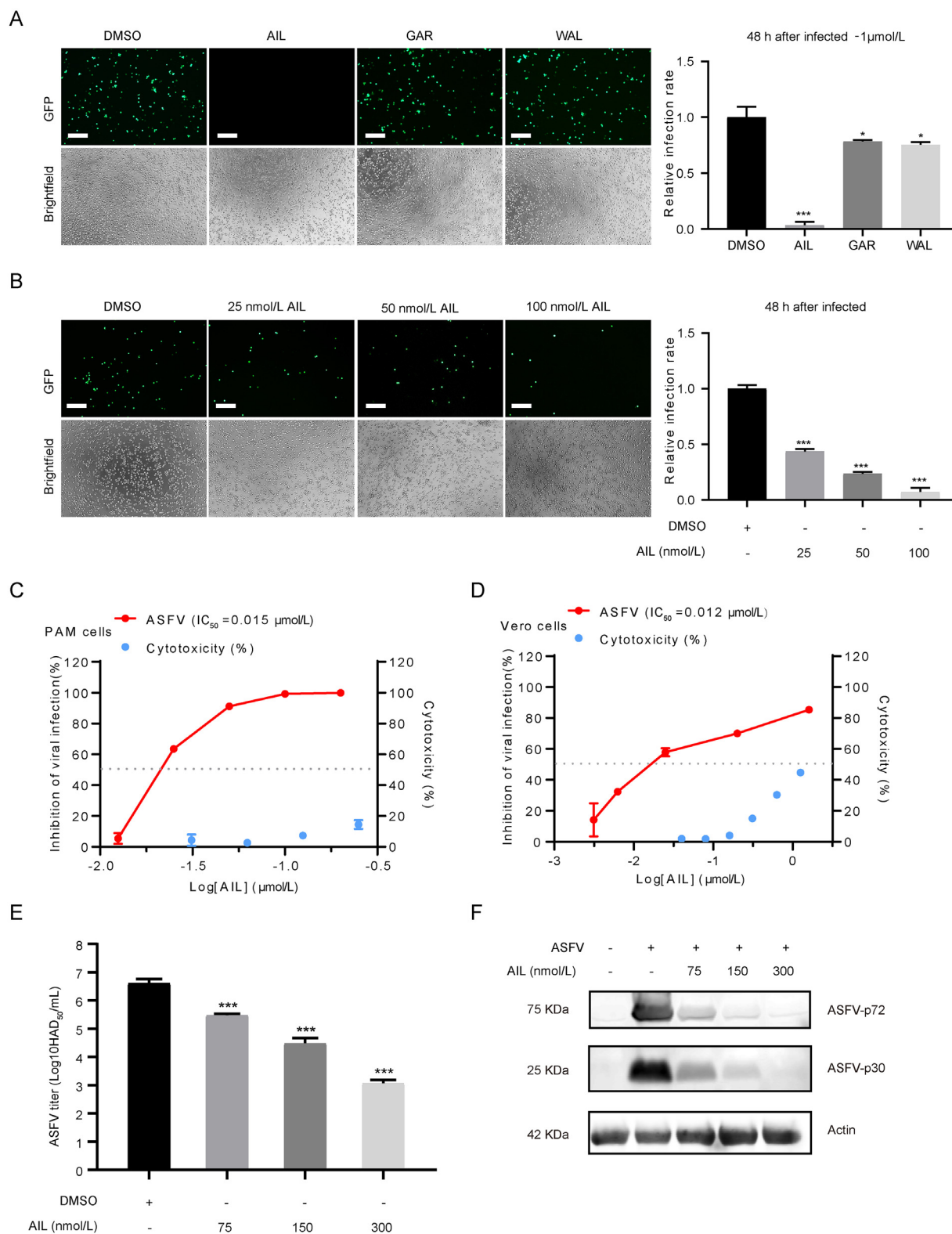
Fig. 4. Ailanthone inhibits the replication of ASFV *in vitro*. **A** Antiviral activity of AIL, GAR and WAL against ASFV-eGFP strains was detected in PAMs by immunofluorescence assay. PAMs (2.5×10^5) were co-incubated with 1 μmol/L AIL, GAR or WAL at 37 °C for 2 h, inoculated ASFV-eGFP (MOI = 0.05) for another 2 h, and then the RPMI 1640 medium within drug was added for 48 h at 37 °C, 5% CO_2. Finally, the brightfield and fluorescence pictures were taken with a fluorescence microscope (**B**). The viral inhibition effect against ASFV-eGFP and cytotoxicity of AIL in PAMs (**C**) or Vero cells (**D**) were analyzed by RT-qPCR and CellTiter-Glo, respectively. (**E & F**) The antiviral effect of AIL on ASFV wild-type strain ASFV-HLJ-2018. PAM cells were treated with different concentrations of AIL after infected by ASFV-HLJ-2018 with MOI at 0.1. The titer of virus was determined by hemadsorption (HAD) assay after 48 h treatment, and 50% HAD doses (HAD_{50}) were calculated by using the method of Reed and Muench. Viral protein synthesis of ASFV-HLJ-2018 were analyzed by Western blotting. Actin was used as a loading control. Scale bar indicated 75 μm. Statistical significance is denoted by *$P < 0.05$, ***$P < 0.001$.

in the p72-Fluc system, and 25 of them were discarded due to their strong cytotoxicity in the follow-up experiments (Table 1). Three compounds stood out with low cytotoxicity and high inhibition of the p72-Fluc system, namely ailanthone (AIL), gartanin (GAR) and walsuralactam A (WAL) (Fig. 3A–C).

3.3. Effect of ailanthone, gartanin and walsuralactam A on the ASFV replication

We used porcine alveolar macrophages (PAMs), the physiological host cells of ASFV, to further verify the inhibitory effects of the three drugs. PAMs were infected with ASFV-eGFP and treated with AIL, GAR or WAL. The fluorescent results indicate only AIL can dramatically suppress the ASFV at 1 μmol/L (Fig. 4A). Therefore, AIL was chosen for further evaluation at lower concentrations. The fluorescence intensity of ASFV-eGFP was significantly decreased in an AIL dose-dependent fashion (Fig. 4B), with an IC_{50} at about 15 nmol/L (Fig. 4C). The cytotoxic effect is very moderate in comparison with CC_{50} higher than 613 nmol/L (Fig. 4C), giving a selectivity index (CC_{50}/IC_{50}) greater than 41. Similarly, the viral infection level in Vero-E6 cells was effectively inhibited at nanomolar concentrations by

AIL ($IC_{50} = 12$ nmol/L) (Fig. 4D). Furthermore, the ASFV-HLJ-2018 strain, which is the circulating strain in China, was adopted to evaluate the antiviral effect of AIL on wild-type strain ASFV. Hemadsorption assay and Western blot assay showed that AIL can potently inhibit the replication of this wildtype ASFV strain HLJ-2018 in a dose-dependent manner (Fig. 4E and F).

3.4. Overexpression of p23 promotes ASFV replication and attenuates the inhibitory effect of ailanthone

AIL has been reported to inhibit the interaction between the HSP90 and its co-chaperone p23 and cause misfolding or degradation of client proteins of HSP90 (He et al., 2016; Bailly, 2020). We found that transient overexpression of p23 mitigated the decrease of p72-Fluc luminescence intensity by AIL treatment, suggesting that p23 attenuated the activity of AIL (Fig. 5A). We further generated a stable cell line which overexpressed p23 and infected it with ASFV-eGFP strain, the fluorescence density was significantly higher in p23-overexpressing group (Fig. 5B). The infection rate was increased by over two-folds due to p23 overexpression (Fig. 5C). These results suggest that p23 facilitates the replication of ASFV and partially rescued the suppressive effect of AIL.
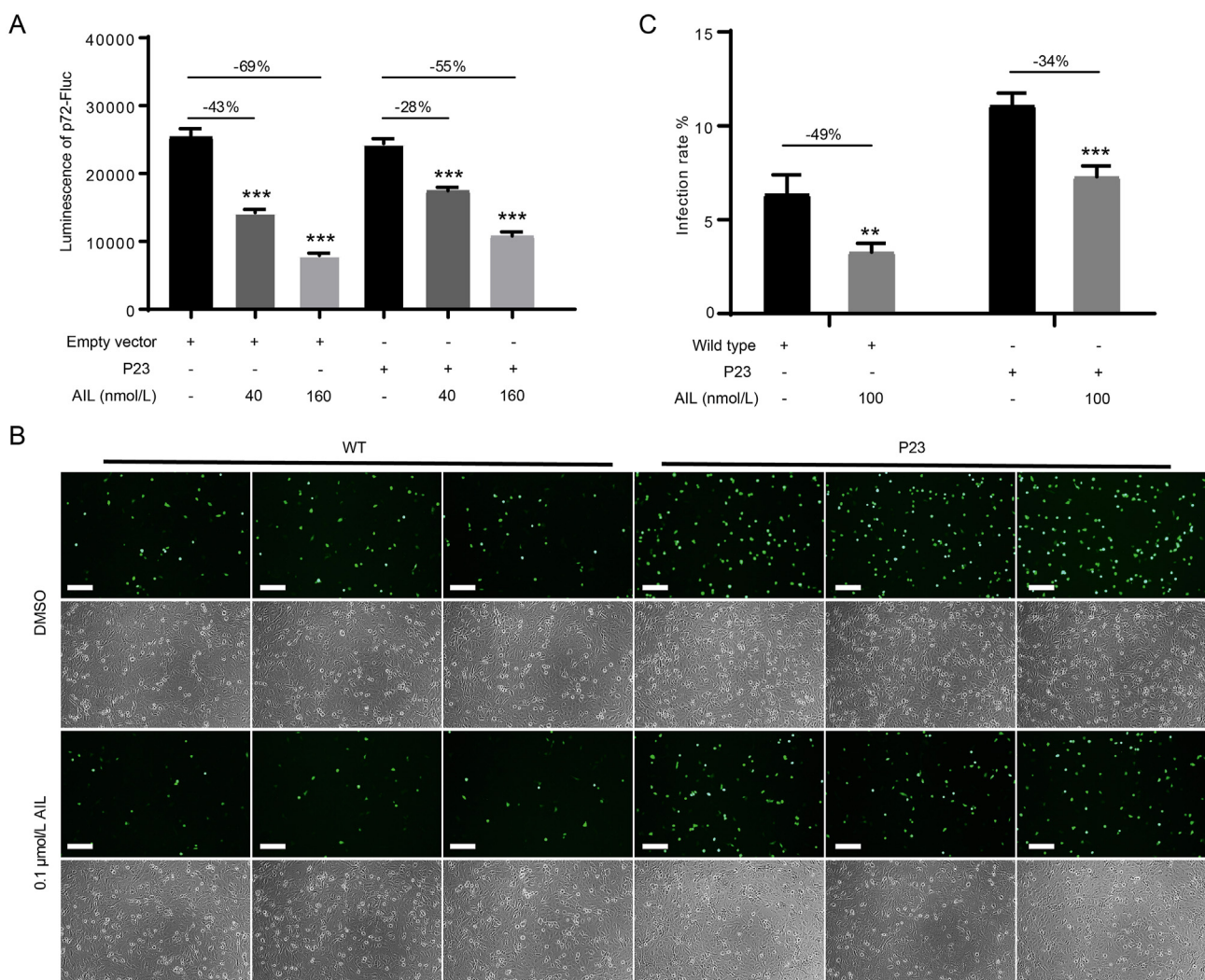

Fig. 5. Overexpression of p23 improves ASFV replication and attenuates the inhibitory effect of ailanthone. **A** Luminescence of p72-Fluc. HEK293T cells (3×10^5) were transfected with 0.5 μg empty vector or p23 plasmids in combination with the p72-Fluc system and then co-incubation with AIL, the luminescence was detected by a multiplate reader. **B** Overexpression of p23 in Vero-E6 cell facilitates the replication of ASFV. Vero-E6 (wildtype) or a stable Vero-E6 cell line which overexpressed p23 were infected with ASFV-eGFP (MOI = 0.1). Two days after infection, the bright field and fluorescence pictures were taken with a fluorescence microscope. Then the infection rate was calculated by ImageJ (**C**). Scale bar: 75 μm. Statistical significance is denoted by **$*P < 0.05$ and **$*P < 0.001$.

3.5. Downregulation of p23 inhibited the ASFV replication

Since overexpression of p23 promoted the replication of ASFV and partially rescued the inhibitory effect of AIL, we downregulated the expression of p23 to further evaluate the relations between p23 and AIL. The luminescence of p72-Fluc was significantly decreased after down-regulating p23 with siRNA or treatment with 400 nmol/L AIL, and even more so after combined treatments of si-P23 and AIL (Fig. 6A). The protein level of ASFV polymerase was significantly reduced following treatment with AIL or siRNA targeting p23, and this inhibition occurred in a dose-dependent manner (Fig. 6B). Furthermore, knockdown p23 or AIL treatment significantly decreased the relative expression of ASFV p72 in ASFV-infected PAMs (Fig. 6C). Both knockdown of p23 and AIL treatment inhibited the luminescence of p72-Fluc as well as replication of ASFV in a similar pattern. These results suggest that p23 is a key factor mediating the inhibitory effect of AIL.

3.6. Ailanthone inhibits Zika virus and hepatitis B virus infection in vitro

HSP90 is a highly conserved and ubiquitous molecular chaperone in eukaryotic cells that is involved in the folding and maturation of hundreds of client proteins (Taipale et al., 2010; Schopf et al., 2017). The p23 is a small but important cochaperone for the HSP90 chaperoning pathway, which binds to the N-terminal domain of HSP90 and stabilizes the closed state of HSP90 to promote client maturation (Ali et al., 2006; Schopf et al., 2017). Several viral proteins have been reported as client proteins of HSP90 chaperone cycle, such as dengue virus, hepatitis B virus, norovirus, influenza virus (Hu and Seeger, 1996; Naito et al., 2007; Vashist et al., 2015; Srisutthisamphan et al., 2018). Since p23 is the target of AIL, we assumed AIL has the potential to be a broad-spectrum antiviral drug and evaluated the antiviral ability with Zika virus and hepatitis B virus (HBV). As expected, viral infection by Zika virus was

significantly inhibited with IC_{50} of 12 nmol/L (Fig. 7A). Immunofluorescence imaging was adapted to further illustrate the inhibitory effect of AIL, the fluorescence density of Zika virus was decreased in a dose-dependent manner (Fig. 7B and C). As a representative of DNA virus, HBV was significantly inhibited by AIL, the relative mRNA level of 3.5 kb HBV was significantly decreased in an AIL dose-dependent manner (Fig. 8A). HBV E protein was further detected by ELISA to quantitate the inhibition of HBV by AIL (Fig. 8B). These results demonstrate the broad antiviral potential of AIL.

4. Discussion

Since the first report of ASF in 1921, this infectious disease has been globally disseminated and caused grave economic losses (Li et al., 2022). ASFV has co-evolved with its host for more than 100 years, and several strains have been studied for decades, unfortunately, there are still no safe and effective drugs against ASFV available. Therefore, it is urgent to identify new effective antiviral drugs for controlling ASFV. Each ASFV particle consists of 8280 copies of the major capsid protein p72, which is encoded by *B646L* gene and is one of the most abundant structural proteins involved in the viral assembly (Liu S. et al., 2019). Since ASFV encodes its own transcriptional machinery, to construct a p72 promoter-driven luciferase reporter system, we need to co-transfect the ASFV RNA polymerase to ensure the operation of viral transcription. And we observed that the intensity of p72-Fluc were remarkably increased after co-transfecting ASFV-RNAP, which is consistent with previous studies (Cackett et al., 2020).

Here, we set up a p72 promoter-driven luciferase reporter system for high throughput screening and verified the reliability and stability of the p72-Fluc system. Our research not only demonstrated the core set of transcriptional machinery of ASFV, but also provided a useful tool for anti-ASFV drug screen. Interestingly, ASFV genome encodes a protein
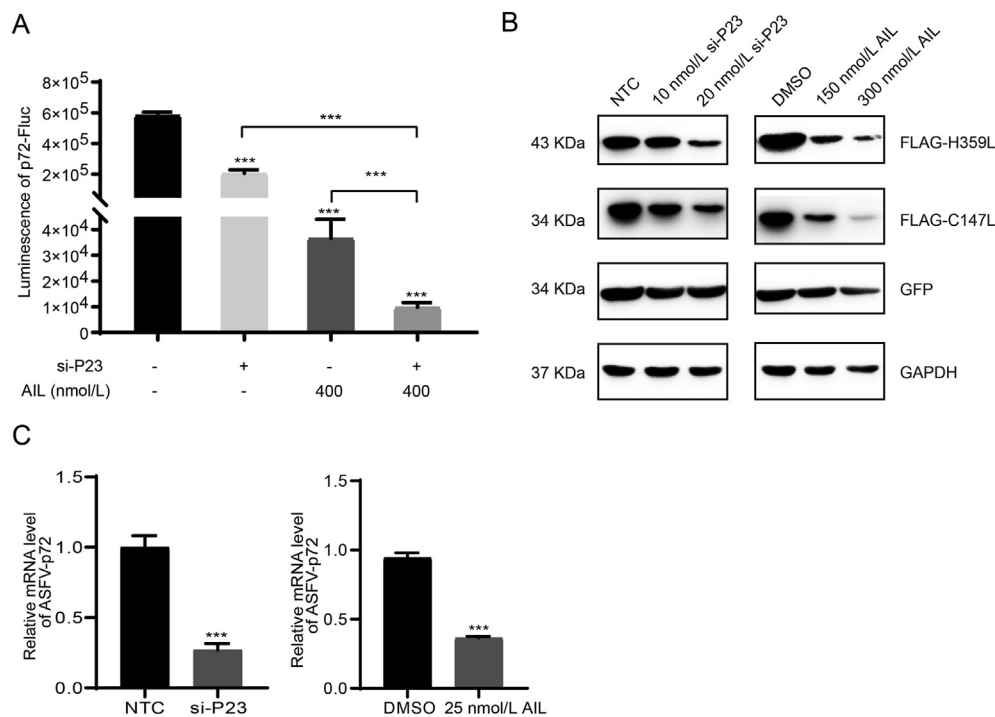

Fig. 6. Downregulation of p23 inhibited the ASFV replication. **A** HEK293T cells were treated with si-p23 or AIL, and then transfected with p72-Fluc system. The luminescence of p72-Fluc were acquired by a multiplate reader. **B** HEK293T cells were transfected with p23 si-RNA or treated with AIL, and then transfected with the ASFV polymerase subunits H359L, C147L or GFP as control. H359L, C147L or GFP were detected by Western blotting. NTC indicated nontargeting control siRNA. **C** PAMs cells were treated with si-p23 or AIL, and then infected with ASFV-eGFP (MOI = 0.1), the relative expression of ASFV-p72 were measured by RT-qPCR at day 2 post-infection. Statistical significance is denoted by ***$P < 0.001$.
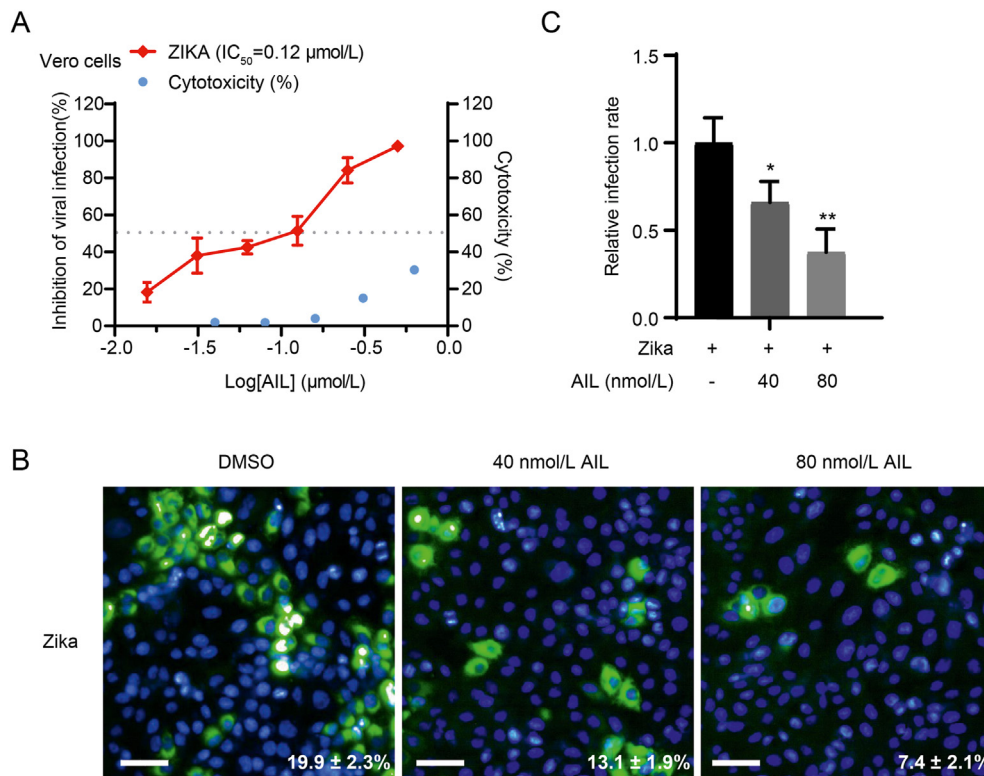
Fig. 7. Ailanthone inhibits the replication of Zika virus *in vitro*. **A** The inhibitory effect of AIL against Zika virus and cytotoxicity of AIL in Vero cells were analyzed by RT-qPCR and CellTiter-Glo. **B** Vero cells were infected with Zika virus (MOI = 0.7), and treated with different concentrations of AIL. The fluorescence images of the viral infections were captured by a microscope. **C** The relative infection rate of Zika virus was calculated by the Harmony high-content imaging and analysis software (Perkinelmer, USA, Opera phenix) according to the manufacturer's instruction. Scale bar indicated 75 μm. Statistical significance is denoted by * $P < 0.05$, and ** $P < 0.01$.
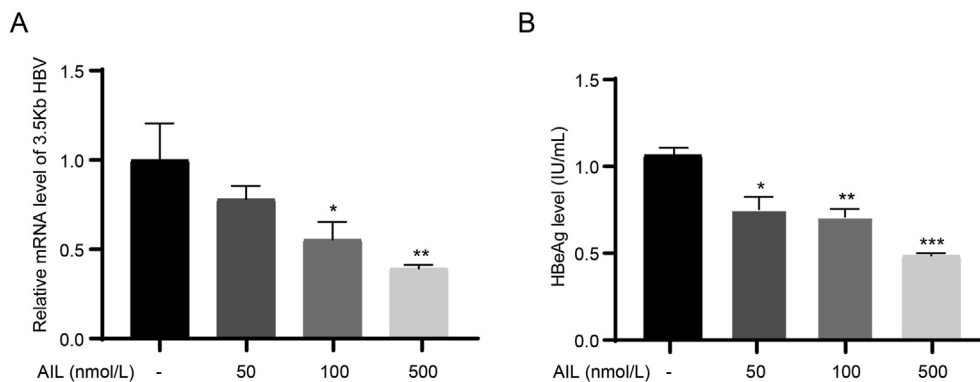

Fig. 8. Ailanthone inhibits the replication of hepatitis B virus *in vitro*. **A** Relative mRNA level of 3.5 kb HBV. HepG2-2B1 cell were infected with HBV (MOI = 100) and treated with different concentrations of AIL. At day 7 post infection, the total RNA was collected for RT-qPCR. **B** Supernatants collected at day 7 post infection were detected by ELISA to quantify HBV e protein antigen level. Statistical significance is denoted by * $P < 0.05$, ** $P < 0.01$ and *** $P < 0.001$.

called D339L that contains a protein-protein interaction strand-helix-strand-strand domain (SHS2), which is similar to the SHS2 domain found in the eukaryotic RNA-polymerase II subunit 7 (RPB7) (Rodríguez and Salas, 2013). RPB7 usually fulfills its function by heterodimerizing with Rpb4. And this heterodimer forms a stalk domain that facilitates the template to insert into the cleft on the structure pol II; nevertheless, this function of RPB4/7 might not be conserved due to that the RBP4 homolog is completely absent in all viral proteins characterized to date (Mirzakhanyan and Gershon, 2017). Furthermore, D339L as ASFV-RPB7 possesses a redundant C-terminus, with no homology to corresponding homolog proteins in host cells (Cackett et al., 2020). Combining our

results that lack of D339L does not decrease the luciferase activity or mRNA expression of p72-Fluc, D339L may not be necessary for our p72-Fluc system. Although we cannot rule out the possibility that D339L is necessary for the transcription of other genes or promoters.

Natural products provide unique and useful resources for drug discovery. In this study, we screened a natural product compound library on our p72-Fluc system and identified three potent candidates which exhibit anti-ASFV effects. Then the *in vitro* experiments further proved that AIL has an antiviral effect at extremely low concentrations. Ailanthone, as a quassinoid extract from the traditional Chinese medicine plant Ailanthus altissima, has been shown to exhibit anti-inflammatory, antimalarial and

antitumor effects (He et al., 2016; Bailly, 2020; Ding et al., 2020). However, to the best of our knowledge, there is no prior study on the antiviral activity of ailanthone. Several studies have reported that AIL targets the p23 to prevent the interaction between client protein and HSP90, thus leading to the degradation of client proteins (He et al., 2016; Tang et al., 2019). Therefore, we suspected that the antiviral effect of AIL may also be dependent on p23. We found that the overexpression of the p23 can facilitate the replication of ASFV and partially rescue AIL-induced reduction of p72-Fluc luminescence. On the other hand, knockdown of p23 decreased the intensity of p72-Fluc and ASFV infection in a similar pattern as AIL treatment. Taken together, our results suggest that the AIL targets p23 to inhibit ASFV replication.

The molecular chaperone p23 is ubiquitously expressed and evolutionarily conserved in eukaryotes; it binds to the HSP90 dimer to maintain the closed conformation of HSP90, thereby promoting the processing and maturation of client proteins (Felts and Toft, 2003). Several previous studies have been published about the relevance of HSP90 to Zika virus and HBV. HSP90 interacts with several flavivirus proteins, and flavivirus nonstructural protein NS5 dysregulates HSP90 to inhibit JAK/STAT signaling (Srisutthisamphan et al., 2018; Taguwa et al., 2019; Roby et al., 2020). HSP90 is essential for the function of HBV reverse transcriptase, in addition, HBV core protein and reverse transcriptase were verified as client proteins of HSP90 (Beck and Nassal, 2003; Hu et al., 2004; Chen et al., 2017). Since the chaperone cycle of HSP90 assists the maturation of hundreds of client proteins and dozens of viral proteins have been reported as client proteins of HSP90 machinery, we speculated that the antiviral effect of AIL is not limited to ASFV. Our results showed the antiviral effect of AIL on Zika virus and HBV, suggesting a broad-spectrum antiviral effect. Future studies on the application of AIL as a broad-spectrum antiviral drug are justified given the lack of such drugs for both human and animal uses.

5. Conclusions

In conclusion, we constructed a p72 promsssssoter-driven luciferase reporter system for high throughput screening, and identified the antiviral effects of AIL on ASFV, Zika virus and HBV. Overexpression of p23 facilitated the replication of ASFV, knockdown of p23 exhibited a similar pattern to AIL treatment, suggesting the AIL targets p23 to inhibit ASFV. To the best of our knowledge, this is the first report on the broad-spectrum antiviral effects of AIL. Future studies may explore the precise molecular mechanism and the clinical effects of AIL as an antiviral agent.

Data availability

Additional data are available from the corresponding author by email request.

Ethics statement

This article does not contain any studies with human subjects. The animal study was reviewed and approved by the Animal Ethics Committee of Hunan Agricultural University and the Animal Care and Use Committee of the Harbin Veterinary Research Institute (HVRI) of the Chinese Academy of Agricultural Sciences (CAAS).

Author contributions

Xu Tan contributed to the conception of the study, funding acquisition, project administration, supervision and writing-review & editing. Xiaofeng Zheng and Dongming Zhao performed the funding acquisition, project administration, supervision and writing-review & editing. Yuhang Zhang performed the experiment, data curation, formal analysis, investigation, validation, visualization and writing-original draft. Zhenjiang Zhang contributed significantly to formal analysis, validation, and

manuscript preparation. Fan Zhang, Nianchao Qian, Jun Jiao, Min Hou and Jiwen Zhang assisted in data curation, formal analysis, investigation, and validation.

Conflict of interest

The authors declare that they have no conflict of interest.

Acknowledgements

Appendix A. Supplementary data

Supplementary data to this article can be found online at https://doi.org/10.1016/j.virs.2023.03.004.

References

Alejo, A., Matamoros, T., Guerra, M., Andrés, G., 2018. A proteomic atlas of the african swine fever virus particle. J. Virol. 92, e01293, 18.

Ali, M., Roe, S., Vaughan, C., Meyer, P., Panaretou, B., Piper, P., Prodromou, C., Pearl, L., 2006. Crystal structure of an Hsp90-nucleotide-p23/Sba1 closed chaperone complex. Nature 440, 1013–1017.

Bailly, C., 2020. Anticancer properties and mechanism of action of the quassinoid ailanthone. Phytother Res. 34, 2203–2213.

Beck, J., Nassal, M., 2003. Efficient Hsp90-independent in vitro activation by Hsc70 and Hsp40 of duck hepatitis B virus reverse transcriptase, an assumed Hsp90 client protein. J. Biol. Chem. 278, 36128–36138.

Cackett, G., Sýkora, M., Werner, F., 2020. Transcriptome view of a killer: African swine fever virus. Biochem. Soc. Trans. 48, 1569–1581.

Chen, W., Zhao, D., He, X., Liu, R., Wang, Z., Zhang, X., Li, F., Shan, D., Chen, H., Zhang, J., Wang, L., Wen, Z., Wang, X., Guan, Y., Liu, J., Bu, Z., 2020. A seven-gene-deleted African swine fever virus is safe and effective as a live attenuated vaccine in pigs. Sci. China Life Sci. 63, 623–634.

Chen, Z., Eggerman, T., Bocharov, A., Baranova, I., Vishnyakova, T., Kurlander, R., Patterson, A., 2017. Heat shock proteins stimulate APOBEC-3-mediated cytidine deamination in the hepatitis B virus. J. Biol. Chem. 292, 13459–13479.

Ding, H., Yu, X., Hang, C., Gao, K., Lao, X., Jia, Y., Yan, Z., 2020. Ailanthone: a novel potential drug for treating human cancer. Oncol. Lett. 20, 1489–1503.

Dixon, L., Chapman, D., Netherton, C., Upton, C., 2013. African swine fever virus replication and genomics. Virus Res. 173, 3–14.

Felts, S., Toft, D., 2003. p23, a simple protein with complex activities. Cell Stress Chaperones 8, 108–113.

Gaudreault, N., Madden, D., Wilson, W., Trujillo, J., Richt, J., 2020. African swine fever virus: an emerging DNA arbovirus. Front. Vet. Sci. 7, 215.

Ge, S., Li, J., Fan, X., Liu, F., Li, L., Wang, Q., Ren, W., Bao, J., Liu, C., Wang, H., Liu, Y., Zhang, Y., Xu, T., Wu, X., Wang, Z., 2018. Molecular characterization of african swine fever virus, China, 2018. Emerg. Infect. Dis. 24, 2131–2133.

He, Y., Peng, S., Wang, J., Chen, H., Cong, X., Chen, A., Hu, M., Qin, M., Wu, H., Gao, S., Wang, L., Wang, X., Yi, Z., Liu, M., 2016. Ailanthone targets p23 to overcome MDV3100 resistance in castration-resistant prostate cancer. Nat. Commun. 7, 13122.

Hu, J., Flores, D., Toft, D., Wang, X., Nguyen, D., 2004. Requirement of heat shock protein 90 for human hepatitis B virus reverse transcriptase function. J. Virol. 78, 13122–13131.

Hu, J., Seeger, C., 1996. Hsp90 is required for the activity of a hepatitis B virus reverse transcriptase. Proc. Natl. Acad. Sci. U. S. A. 93, 1060–1064.

Li, P., Wei, Y., Mei, M., Tang, L., Sun, L., Huang, W., Zhou, J., Zou, C., Zhang, S., Qin, C., Jiang, T., Dai, J., Tan, X., Zhang, Q., 2018. Integrative analysis of Zika virus genome RNA structure reveals critical determinants of viral infectivity. Cell Host Microbe 24, 875–886.e875.

Li, Z., Chen, W., Qiu, Z., Li, Y., Fan, J., Wu, K., Li, X., Zhao, M., Ding, H., Fan, S., Chen, J., 2022. African swine fever virus: a review. Life 12, 1255.

Liu, Q., Ma, B., Qian, N., Zhang, F., Tan, X., Lei, J., Xiang, Y., 2019a. Structure of the African swine fever virus major capsid protein p72. Cell Res. 29, 953–955.

Liu, S., Luo, Y., Wang, Y., Li, S., Zhao, Z., Bi, Y., Sun, J., Peng, R., Song, H., Zhu, D., Sun, Y., Li, S., Zhang, L., Wang, W., Sun, Y., Qi, J., Yan, J., Shi, Y., Zhang, X., Wang, P., Qiu, H., Gao, G., 2019. Cryo-EM structure of the african swine fever virus. Cell Host Microbe 26, 836–843.e833.

Malmquist, W., Hay, D., 1960. Hemadsorption and cytopathic effect produced by African Swine Fever virus in swine bone marrow and buffy coat cultures. Am. J. Vet. Res. 21, 104–108.

Mirzakhanyan, Y., Gershon, P., 2017. Multisubunit DNA-dependent RNA polymerases from Vaccinia virus and other nucleocytoplasmic large-DNA viruses: impressions from the age of structure. Microbiol. Mol. Biol. Rev. 81, e00010, 17.

Naito, T., Momose, F., Kawaguchi, A., Nagata, K., 2007. Involvement of Hsp90 in assembly and nuclear import of influenza virus RNA polymerase subunits. J. Virol. 81, 1339–1349.

Reed, L.J., Muench, H., 1938. A simple method of estimating fifty per cent ENDPOINTS12. Am. J. Epidemiol. 27, 493–497.

Roby, J., Esser-Nobis, K., Dewey-Verstelle, E., Fairgrieve, M., Schwerk, J., Lu, A., Soveg, F., Hemann, E., Hatfield, L., Keller, B., Shapiro, A., Forero, A., Stencel-Baerenwald, J., Savan, R., Gale, M., 2020. Flavivirus nonstructural protein NS5 dysregulates HSP90 to broadly inhibit JAK/STAT signaling. Cells 9, 899.

Rodríguez, J., Salas, M., 2013. African swine fever virus transcription. Virus Res. 173, 15–28.

Schopf, F., Biebl, M., Buchner, J., 2017. The HSP90 chaperone machinery. Nat. Rev. Mol. Cell Biol. 18, 345–360.

Srisutthisamphan, K., Jirakanwisal, K., Ramphan, S., Tongluan, N., Kuadkitkan, A., Smith, D., 2018. Hsp90 interacts with multiple dengue virus 2 proteins. Sci. Rep. 8, 4308.

Taguwa, S., Yeh, M., Rainbolt, T., Nayak, A., Shao, H., Gestwicki, J., Andino, R., Frydman, J., 2019. Zika virus dependence on host Hsp70 provides a protective strategy against infection and disease. Cell Rep. 26, 906–920.e903.

Taipale, M., Jarosz, D., Lindquist, S., 2010. HSP90 at the hub of protein homeostasis: emerging mechanistic insights. Nat. Rev. Mol. Cell Biol. 11, 515–528.

Tang, S., Ma, X., Lu, J., Zhang, Y., Liu, M., Wang, X., 2019. Preclinical toxicology and toxicokinetic evaluation of ailanthone, a natural product against castration-resistant prostate cancer, in mice. Fitoterapia 136, 104161.

Vashist, S., Urena, L., Gonzalez-Hernandez, M., Choi, J., De Rougemont, A., Rocha-Pereira, J., Neyts, J., Hwang, S., Wobus, C., Goodfellow, I., 2015. Molecular chaperone Hsp90 is a therapeutic target for noroviruses. J. Virol. 89, 6352–6363.

Wang, N., Zhao, D., Wang, J., Zhang, Y., Wang, M., Gao, Y., Li, F., Wang, J., Bu, Z., Rao, Z., Wang, X., 2019. Architecture of African swine fever virus and implications for viral assembly. Science 366, 640–644.

Wang, Y., Kang, W., Yang, W., Zhang, J., Li, D., Zheng, H., 2021. Structure of african swine fever virus and associated molecular mechanisms underlying infection and immunosuppression: a review. Front. Immunol. 12, 715582.

Xiang, C., Du, Y., Meng, G., Soon Yi, L., Sun, S., Song, N., Zhang, X., Xiao, Y., Wang, J., Yi, Z., Liu, Y., Xie, B., Wu, M., Shu, J., Sun, D., Jia, J., Liang, Z., Sun, D., Huang, Y., Shi, Y., Xu, J., Lu, F., Li, C., Xiang, K., Yuan, Z., Lu, S., Deng, H., 2019. Long-term functional maintenance of primary human hepatocytes in vitro. Science 364, 399–402.

You, S., Liu, T., Zhang, M., Zhao, X., Dong, Y., Wu, B., Wang, Y., Li, J., Wei, X., Shi, B., 2021. African swine fever outbreaks in China led to gross domestic product and economic losses. Nature Food 2, 802–808.

Zhao, D., Liu, R., Zhang, X., Li, F., Wang, J., Zhang, J., Liu, X., Wang, L., Zhang, J., Wu, X., Guan, Y., Chen, W., Wang, X., He, X., Bu, Z., 2019. Replication and virulence in pigs of the first African swine fever virus isolated in China. Emerg. Microb. Infect. 8, 438–447.

Zheng, X., Nie, S., Feng, W.H., 2022 Apr. Regulation of antiviral immune response by African swine fever virus (ASFV). Virol. Sin. 37, 157–167.

Zhou, X., Li, N., Luo, Y., Liu, Y., Miao, F., Chen, T., Zhang, S., Cao, P., Li, X., Tian, K., Qiu, H., Hu, R., 2018. Emergence of african swine fever in China, 2018. Transbound Emerg Dis 65, 1482–1484.